Journal of Medical Systems (2018) 42: 134
https://doi.org/10.1007/s10916-018-0989-3

IMAGE & SIGNAL PROCESSING

False Positive Reduction by an Annular Model as a Set of Few Features for Microcalcification Detection to Assist Early Diagnosis of Breast Cancer

Jonathan Hernández-Capistrán[1] · Jorge F. Martínez-Carballido[1] · Roberto Rosas-Romero[2]

Received: 25 March 2018 / Accepted: 7 June 2018 / Published online: 18 June 2018

Abstract
Early automatic breast cancer detection from mammograms is based on the extraction of lesions, known as *microcalcifications* (MCs). This paper proposes a new and simple system for *microcalcification detection* to assist in early breast cancer detection. This work uses the two most recognized public mammogram databases, MIAS and DDSM. We are introducing a MC detection method based on (1) Beucher gradient for detection of *regions of interest* (ROIs), (2) an annulus model for extraction of few and effective features from candidates to MCs, and (3) one classification stage with two different classifiers, *k Nearest Neighbor* (KNN) and *Support Vector Machine* (SVM). For dense mammograms in the MIAS database, the performance metrics achieved are *sensitivity* of 0.9835, *false alarm rate* of 0.0083, *accuracy* of 0.9835, and *area under the ROC curve* of 0.9980 with a KNN classifier. The proposed MC detection method, based on a KNN classifier, achieves, a *sensitivity*, *false positive rate*, *accuracy* and *area under the ROC curve* of 0.9813, 0.0224, 0.9795 and 0.9974 for the MIAS database; and 0.9035, 0.0439, 0.9298 and 0.9759 for the DDSM database. By slightly reducing the true positive rate the method achieves *three instances with false positive rate of 0*: 2 on fatty mammograms with KNN and SVM, and one on dense with SVM. The proposed method gives better results than those from state of the art literature, when the mammograms are classified in *fatty, fatty-glandular,* and *dense*.

Keywords Digital mamograms,microcalcifications · K-nearest neighbors · Support vector machine · Morphologic image processing · Feature extraction

Introduction

Breast cancer is the number one cause of deaths in women and it corresponds to approximately 15% of all cancer deaths among women. Worldwide, 570,000 women died of breast cancer in 2015 [1].

Numerous experiments have established that an early detection of cancer eases the treatment, reducing risks, as well as the mortality percentage in 25% [2]. For early detection, *mammography* is an imaging tool with high sensitivity and it is the most recommended by the guidelines of the World Health Organization [3, 4].

A mammogram is the best diagnostic tool to find a cluster of microcalcifications (MCs) in a glandular duct. MCs appear as white specks [5], and they are early signs of breast cancer. Microcalcification lesions are difficult to detect by human vision since microcalcification size is between 0.5 to 2 mm. For this reason, the *false positive rate* of a radiologist is reported at 15% [6] and the *false negative rate* at 20% [7].

This work proposes an algorithm, which detects microcalcifications on mammograms based on morphologic processing, learning machines and a very small set of features. These arguments encourage the implementation of autonomous diagnostic tools to detect early risks of breast cancer by finding

This article is part of the Topical Collection on *Image & Signal Processing*

✉ Jonathan Hernández-Capistrán
jhcapistran@gmail.com

Jorge F. Martínez-Carballido
jmc@inaoep.mx

Roberto Rosas-Romero
roberto.rosas@udlap.mx

[1] Instituto Nacional de Astrofísica, Óptica y Electrónica, Luis Enrique Erro # 1, Santa María Tonantzintla, 72840 Puebla, Pue, Mexico

[2] Universidad de las Américas-Puebla, San Andrés, Cholula, Puebla, Mexico

the presence of MCs on mammograms so that patients can follow specialized treatment.

Related work

The work in [8], proposed a microcalcification detecting system which applies a Swarm Optimization Neural Network (SONN). Features applied to this classifier were extracted using texture energy measures obtained through a convolutional kernel. The method in [9] proposed a biological adaptive model of contrast detection. This model is based on the human visual system (HSV) to adapt the contrast according to the HSV model. Before applying this model, the image is filtered based on anisotropic diffusion and curvilinear structure using local energy and phase congruency. The aim is to reduce false positives due shot noise or curvilinear structures. In another method [10], the microcalcification segmentation is based on the geodesic active contours (GAC) technique associated with anisotropic texture filtering. Authors of [11] proposed microcalcification detection using the two-dimensional discrete wavelet transform. Before segmenting the region of interest, an enhacement step is applied by Logarithm transformation for dynamic range manipulation. To extract ROIs, a binarization step with automatic threshold and morphological operations are applied; followed by unsharp masking to enhace the ROI. As a final step, a discrete Wavelet transform is applied to detect microcalcifications.

Previous works are characterized by the classifier and database that are used to test the proposed approach. Well known public databases are *Digital Mammogram Database*, (MIAS) [12] and the *Digital Database for Screening Mammography*, (DDSM) [13]. Works that have used only one of these databases are: [6, 8, 9, 11, 14]. Works that used both datasets are [17, 19–21]. Some works did not use a public database such as [10, 15, 16]. Methods based on KNN classifiers are found in [16–18] and those based on SVM are found in [8, 16, 19]. Both classifiers are used in [16]. Other classifiers used for MC detection are Fuzzy C-means with Features (FCM-WF) [15] and Adaboost [6].

From this analysis, it is observed that there are significant differences in terms of databases and the number of images used by each method. One difficulty is that different works do not specify what images of the database were used so that it is not possible to tell if hard images are taken out of the testing set, thus making any comparison unfair. Six of the reviewed works on Table 3, do not specify which images left off from their analysis.

This work improves over current state of the art on significant reduction of false positives on dense mammograms by using an annulus model and a set of few features that leads to an overall improved method to detect microcalcifications on mammograms, compared to previous work.

Material and methods

Mammogram databases

We use the two most popular public databases MIAS [12], and DDSM [13]. The first database contains 322 medio–lateral (MLO) mammograms at a spatial resolution of 50 *μm/pixel* and 8 *bits/pixel*. Mammograms are also classified in terms of *breast density type*; *fatty*, *fatty-glandular*, and *dense*. As it is shown in the Table 1, this database contains 207 *normal images (*without microcalcification clusters*)* and 20 images with *clusters of microcalcifications (5 fatty, 6 fatty-glandular, 9 dense)*. Images with microcalcifications are provided along with their corresponding *Ground Truth* (GT), while normal images do not have GTs. The ground truth specifies information regarding ROIs which are *clusters with microcalcifications*. Those 20 images, with specified ground truth, contain 25 regions of interest which include *microcalcification clusters*. From these 25 ROIs, 268 individual microcalcifications were extracted as it is explained in the section "Microcalcification Extraction". Three images (1 fatty, 1 fatty-glandular, and 1 dense) have no clusters of microcalcifications, thus they have no Ground Truth specified; only distributed isolated microcalcifications and that is why they are not considered for analysis. The remaining images from the database correspond to images with other type of lesions without microcalcifications.

The DDSM database was digitized by four different scanners. Table 2 shows information related to this database. This Table does not contain the same type of detailed information as Table 1 because DDSM images in the database do not include breast density type.

Generation of candidates without microcalcifications

The aim of this part of the method is to generate a training set of 21 × 21-pixel image patches, which correspond to candidates. The number of patches with microcalcifications (candidates to be detected as True Positives) is the same as the number of patches without microcalcifications (candidates to be detected as True Negatives).

To generate patches without microcalcifications, normal images are randomly selected, and from each randomly selected normal image a patch is randomly extracted. Each normal image is tagged with a number, and to generate a set of randomly selected normal images, n random *image tags* are generated by means of a *discrete uniform probability density function*, $f(x) = 1/m$; where $x \in \{1, 2, \ldots, m\}$ is an *image tag number*; and m is the total number of images from each mammogram density. Parameters, (n, m), are $(n = 121, m = 76)$, $(n = 97, m = 65)$ and $(n = 50, m = 66)$ for *dense*, *fatty-glandular* and *fatty* mammograms, respectively. For each mammogram density parameter n is chosen so that the number of candidates, which are MCs, is the same as the number of

Table 1 MIAS breast density

MIAS database				
	Fatty	*Fatty-glandular*	*Dense*	Total
Number of images with clusters of microcalcification	5	6	9	20
Images with isolated microcalcifications	1	1	1	3
Number of clusters in GT Images	5	6	14	25
Extracted microcalcifications	50	97	121	268
Images without microcalcification clusters	66	65	76	207

candidates, which are not. According to Table 2, there are 121 MCs in 9 dense mammograms, 97 MCs in 6 fatty-glandular mammograms, and 50 MCs in 5 fatty mammograms.

Similarly, one pair of random numbers, (r, c), is generated for each randomly selected normal image. Parameters r and c are coordinates of the center of a randomly chosen 21×21-pixel patch on the given mammogram.

Ground truth region extraction

The proposed approach, to solve the problem of detecting *microcalcifications* (MC), is separated into three main stages, extraction of abnormal clusters or regions of interest, extraction of individual candidates from abnormal clusters, and classification of candidates.

Extraction of abnormal regions of interests provided by GT images of the database which were specified by a radiologist, by giving (1) coordinates (x, y) of the center of each cluster of interest, and (2) an approximate radius, in pixels, of a circle enclosing an abnormal cluster, as it is shown in Fig. 1. Rather than enclosing a cluster by a circle (Fig. 1 b), a square is used (Fig. 1 c).

Extraction of microcalcifications candidates from abnormal clusters

Extraction of microcalcifications, from an abnormal cluster, is separated into 4 stages: *segmentation* (Beucher Gradient and Enhancement of Gradient Image), *binarization*, *feature extraction*, and *classification*. Fig. 2 shows a mammogram region after different operations are applied to detect microcalcifications.

Table 2 DDSM for abnormality

DDSM		
	Abnormal	Normal
Images	29	20
Extracted microcalcifications	114	114

Segmentation

Microcalcification clusters are obtained from the GT where regions with microcalcifications are specified. These clusters are regions of different sizes. The first two blocks (Original image and Ground Truth region extraction), in Fig. 2, correspond to the mammogram along with a MC cluster specified by the GT, and the purpose of segmentation block is to localize must changing borders. This is accomplished in two steps: Beucher Gradient application and enhancement of gradient image.

Beucher gradient

Because of the fact that *dilation* of gray-level images enhances bright regions and suppresses dark regions while *eroding* enhances dark regions and suppresses bright regions, where the area of the suppressed region is smaller than that of the specified *structuring element* $b(r, c)$, both operations are combined, through the use of the high-pass filter, *Beucher Gradient* [22]. The *erosion* of a gray-level image $f(r, c)$ by a *structuring element* $b(r, c)$ at location (r, c) is obtained by selecting the minimum value of $f - b$ inside the region of intersection over which both functions f and b are defined according to

$$[f \ominus b](r,c) = \min_{(x,\ y) \in b} \{f(r-x, c-y) - b(x,\ y)\} \tag{1}$$

The *dilation* of a gray-level image $f(r, c)$ by a structuring element $b(r, c)$ at location (r, c) is defined by finding the maximum value of $f + b$ inside the common region between both, function f and structuring element b, according to

$$[f \oplus b](r,c) = \max_{(x,y) \in b} \{f(r-x, c-y) + b(x,\ y)\} \tag{2}$$

By considering flat structuring elements with zero entries, *eroding* or *dilating* of a gray-level image with a structuring element consists in finding the *minimum* or *maximum* value of the image inside the region bounded by the intersection of the image and the structuring element.

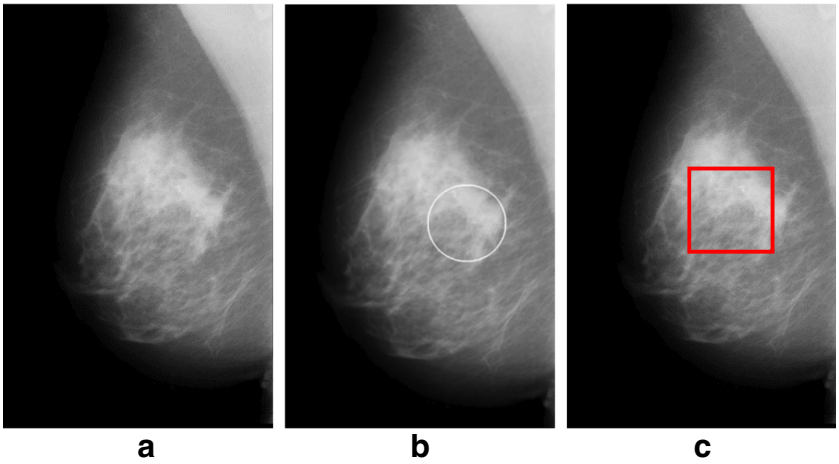

Fig. 1 **a** Digital mammogram from MIAS; **b**) Ground Truth with a white circle enclosing cluster of microcalcifications; **c**) Ground Truth with a red square enclosing a cluster of microcalcifications

The morphological gradient, *Beucher Gradient*, is the arithmetic difference between the dilated and the eroded version of the gray level image of interest $f(r, c)$, by a *structuring element* $b(r, c)$,

$$g(f(r,c)) = [f \oplus b](r,c) - [f \ominus b](r,c) \quad (3)$$

The result of applying Beucher Gradient on a mammogram is shown in the upper right part of Fig. 2.

Enhancement of gradient image

To improve the quality of the filtered image, a 3×3 *median filter* is applied, a non-linear filtering technique to remove

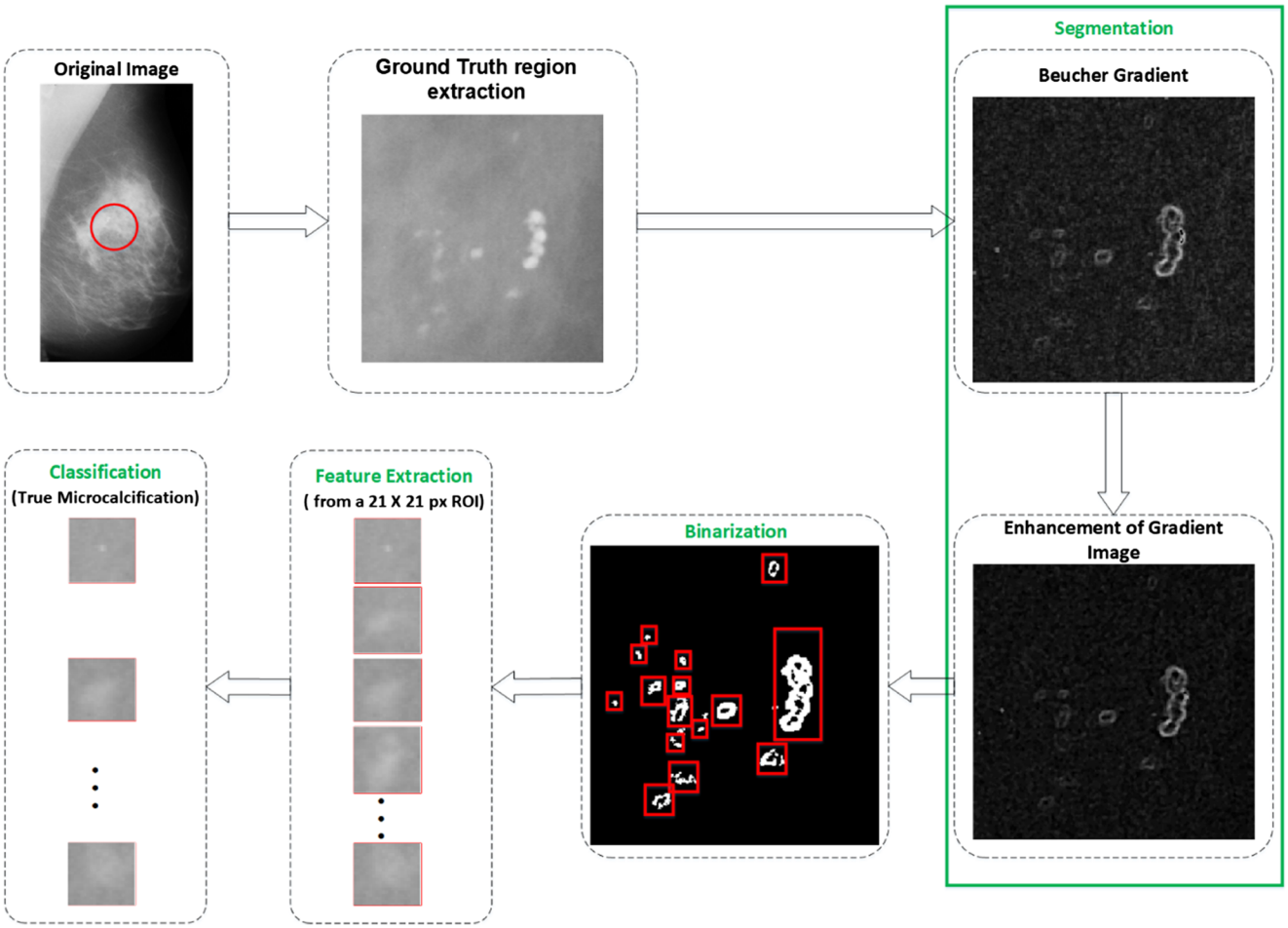

Fig. 2 Microcalcifications cluster, segmentation, binarization, feature extraction, and classification

noise while preserving edges. To enhance edges, a process, called *unsharp masking*, is applied, where a *smoothed* version of the image, $f_{smooth}(r, c)$, is subtracted from the original image, subtracting away the low-frequency components of the signal, and yielding the high-frequency content,

$$f_{high-pass}(r, c) = f(r, c) - f_{smooth}(r, c) \quad (4)$$

where the high-pass image component can be used for sharpening by adding it to the original image. Thus, the complete *unsharp masking* operator is given by

$$f_{sharpen}(r, c) = f(r, c) + A \times f_{high-pass}(r, c) \quad (5)$$

where A is a scaling constant, set to 0.7. The result of applying *median filtering*, followed by *unsharp masking* is shown in the lower right part of Fig. 2.

Binarization

Thresholding is applied to generate a binary image as it is depicted in the block of binarization of Fig. 2. The MC are characterized by abrupt border changes, the enhanced gradient image of the segmentation block represents these changes; thus, the top 10% of the gradient values are most probable to represents MC borders. Therefore, the threshold value, for binarization, is established at 90% of the highest gray value of the enhanced GT region of interest.

One impairment of binarization is that remaining noise might be misclassified as a candidate to microcalcifications. To reduce the likelihood of the occurrence of these misclassifications, ROIs, with radii smaller than 0.1 mm, are eliminated using *opening* with a disk-like structural element of 0.2-mm diameter. The reason for choosing a structuring element of 0.2-mm diameter is based on the consideration that the diameter, of the smallest microcalcification, is 0.2 mm. The *opening* of a binary image $f(r, c)$, by a structuring element $b(x, y)$, is given by $f \circ b = (f \ominus b) \oplus b$, and it eliminates objects smaller than the structuring element. Resolution of digital mammograms, for both databases, is 50 μm per pixel. Thus, the size of the structuring element, in pixels, is $\frac{0.2\ mm/diameter}{50\ \mu m/pixel} = 4\ \frac{0.2\ mm/diameter}{50\ \mu m/pixel}$

Another consideration is that the diameter, of the largest microcalcification, is 1 mm. Thus, the size of the circle, which encloses a candidate to microcalcification, is $\frac{1\ mm/diameter}{50\ \mu m/pixel} = 20\ \frac{1\ mm/diameter}{50\ \mu m/pixel}$, and the area of the corresponding square is chosen as 21×21 pixels. Each MC candidate is in a 21×21 image patch and its center is established at the position of the highest gray level value.

To recover the complete shape of candidates, at all locations of interest, an algorithm for *extraction of connected components* is used. Another motivation for extraction of connected components is to assign a label to each region of interest for sub-sequent automatic extraction of *properties* from each labeled ROI, mainly the position of the highest gray level value inside the region.

Feature extraction

Also, in the feature extraction block of Fig. 2 it is shown the *extraction of features* from a candidate to microcalcification. It is useful to visualize a microcalcification in the three-dimensional space, as a gray level function of coordinates (x, y), as it is observed in Fig. 3. This three-dimensional reconstruction provides an approximation of the projection of an actual microcalcification into a set of intensity values on a digital mammogram. The three-dimensional reconstruction of a microcalcification consists of a prominent peak in relation to local surroundings on the mammogram. Thus, it is feasible the modeling of a microcalcification based on a *set of surface levels*.

To detect real microcalcifications, four features are extracted from a candidate. Information is obtained from three different *surface levels* assigned to each ROI, by using a *mask*, which contains the distribution of these surface levels. Fig. 4 a) shows a ROI with 21 X 21 pixels and with its center at the maximum intensity value. Information, for each surface level of the ROI, is extracted by overlapping the ROI with a mask which shows the distribution of each of the three surface levels. Fig. 4 b) shows the mask along with the distribution of each surface level. The surface level distribution consists of three *concentric annuli* with respective radii R, $R+2$ and $R+4$. This work uses $R=3$, by considering known sizes of microcalcifications. Each *annular region*, $A_{annulus}$, provides information of interest regarding each *surface level*. Each annular region is labeled by an integer number in $\{1, 2, 3\}$.

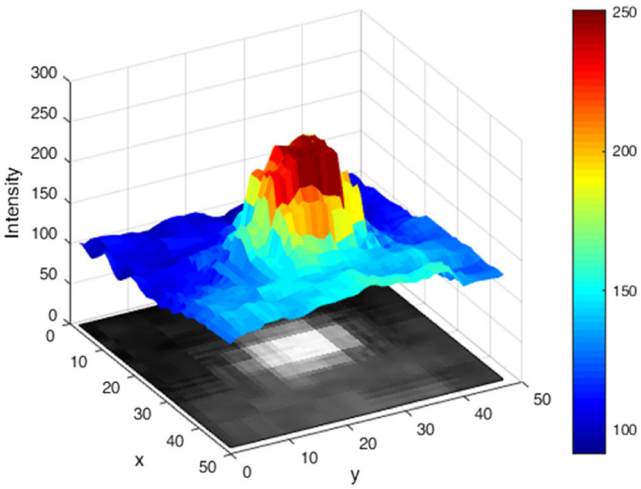

Fig. 3 Visualization of one microcalcification

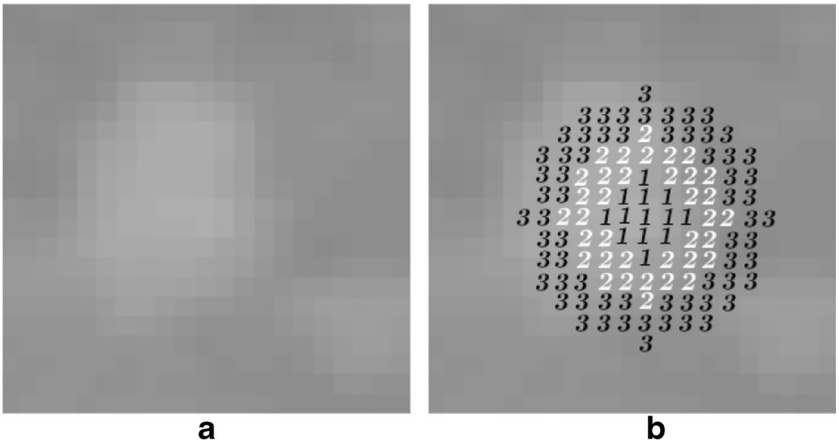

Fig. 4 **a** Region of interest **b**) with corresponding annulus mask

After overlapping the mask with one ROI, information from the three annular regions is used for extraction of a four-entry feature vector, $\boldsymbol{f} = [f_1, f_2, f_3, f_4]^T$, according to,

$$f_1 = max(A_{annulus1}) - max(A_{annulus2}) \quad (6a)$$

$$f_2 = max(A_{annulus1}) - max(A_{annulus3}) \quad (6b)$$

$$f_3 = mean(A_{annulus1}) - mean(A_{annulus2}) \quad (6c)$$

$$f_4 = entropy(A_{annulus1}) - entropy(A_{annulus2}) \quad (6d)$$

where functions *max*(), *mean*(), and *entropy*() are the *maximum*, *mean* and *entropy* values, respectively, of the corresponding annular region intensity values.

The first and the second feature f_1, f_2, represents the difference between the peak intensity value, in the first annular region, and the peak, on the second and third annulus, respectively. For the third feature, f_3, is the difference between first and second mean values. Another feature is the entropy value.

Classification

The classification of true microcalcifications is depicted in the classification block of Fig. 2. To decide whether a ROI is a microcalcification or not, the classifier is implemented by using KNN and SVM.

KNN classifier

The KNN is a non-linear classifier. To assign a class to an unknown feature vector $\boldsymbol{x}$, K feature vectors, out of set of N training feature vectors $\{\boldsymbol{x}_i; i = 1, \ldots, N\}$, are identified as the nearest neighbors to the unknown $\boldsymbol{x}$. Each one of the *k nearest neighbors*, $\boldsymbol{x}_i$, belongs to a corresponding class, C_i, where the number of classes is two (*normal* and *abnormal*). Out of the K *nearest neighbors* to $\boldsymbol{x}$, the number of *nearest neighbors*, k_i, that belong to class C_i ($i = 1, 2$), are identified, where $k = k_1 + k_2$. The class, assigned to $\boldsymbol{x}$, is the one with the largest k_i.

SVM classifier

An SVM is an optimal classifier which is geometrically represented by a separating hyperplane which is the furthest away from each class after training this classifier with labeled data. The *SVM*, in this work, used a *Gaussian Kernel function*, with (1) one output, which provides two possible outcomes, corresponding to two different classes (*microcalcification* or *abnormal region, normal region*), and (2) four inputs according to the size of the feature vector used.

Performance evaluation

To compare works that detect microcalcifications, it is essential to compare efficiency among different proposed methods. To evaluate the performance of the proposed method, *True Positive Rate* (TPR) or *sensitivity*, *False Positive Rate* (FPR), *specificity* and *accuracy* are used as figures of merit. TPR, also known as *sensitivity* or *recall* or *detection alarm*, is the probability that the outcome of a diagnosis is positive given that the patient presents breast cancer, and it is given as,

$$TPR = \frac{TP}{TP + FN} \quad (7)$$

where *true positives* (TP) are those microcalcifications correctly identified and *false negatives* (FN) are those microcalcifications incorrectly rejected. *False Positive Rate* (FPR), also known as *false alarm*, is defined as the probability that the outcome of a breast cancer diagnosis is *positive* given that the patient is healthy according to

$$FPR = \frac{FP}{TN + FP} \quad (8)$$

where *true negatives* (TN) are those cases correctly rejected and *false positives* (FP) are those artifacts incorrectly detected

Table 3 Performance of different methods for microcalcification detection

Ref.	TPR	FPR	Accuracy	AUC	Database	Number of images
[9]	1	0.5			DDSM	58 cluster abnormalities 24 normal
[8]	0.95	0.077		SVM 0.8755	MIAS	216 mammograms
[20]	0.9810	0.63 per image			DDSM MIAS	20 MIAS images. 140 DDSM images.
[17]			MIAS KNN: 0.95 DDSM KNN: 0.86	MIAS KNN: 0.96 DDSM KNN: 0.90	DDSM MIAS	MIAS: 20 patches DDSM: 300 patches
[6]	0.8715	0.0642	0.9143	0.9036	MIAS	208 benign images 80 abnormal images
[14]	0.957		0.959	0.97	MIAS	23 mammograms (7 Glandular, 10 Dense, 6 Fatty) containing microcalcification clusters. 50 mammograms (15 Glandular, 20 Dense, 15 Fatty) without microcalcifications.
[19]	KNN: 0.89 MIAS	KNN: 0.19 MIAS		MIAS SVM: 0.9851 KNN: 0.9256	DDSM MIAS	MIAS 26 ROIs DDSM 103 ROIs
[21]	0.97	0.45 per image			MIAS USCF DDSM	MIAS and UCSF 189 images DDSM 27 abnormal – 18 normal.
[11]	93.1	0.1			MIAS	40 normal 29 microcalcifications
Proposed KNN Proposed SVM Proposed MIAS fatty-glandular Proposed MIAS fatty Proposed MIAS dense 	0.9035 0.9813 0.9424 0.9211 0.9664 0.9476 KNN: 0.9897 SVM: 0.9691 KNN: 0.9400 SVM: 0.9200 KNN: 0.9835 SVM: 0.9752	0.0439 0.0224 0.0497 0.0526 0.0299 0.0550 KNN: 0.0200 SVM: 0.0309 KNN: 0 SVM: 0 KNN: 0.0083 SVM: 0	0.9298 0.9795 0.9463 0.9342 0.9683 0.9463 KNN: 0.9845 SVM: 0.9691 KNN: 0.97 SVM: 0.96 KNN: 0.9835 SVM: 0.9876	0.9759 0.9974 0.9807 0.9656 0.9934 0.9802 KNN: 0.9978 SVM: 0.9930 KNN: 0.9924 SVM: 0.9928 KNN: 0.9980 SVM: 0.9951	DDSM MIAS Both DDSM MIAS Both	MIAS: 20 abnormal images. 207 normal images. ROIs of 21 X 21 pixels: MIAS database 268 normal candidates and 268 microcalcifications. DDSM: 114 normal candidates 114 microcalcifications

as microcalcifications. *Specificity* is defined as $1 - FPR$.

Accuracy specifies the percentage of breast cancer diagnosis which are correct,

$$Accuracy = \frac{TP + TN}{TP + TN + FP + FN} \quad (9)$$

The *receiver operating characteristic* (ROC) curve compares operating characteristics, TPR vs. FPR by plotting them at different plotting settings. The *area under the curve* (AUC) is equal to the probability that a classifier ranks a randomly chosen positive higher than a randomly chosen negative one.

Cross-validation is *k-fold Cross Validation* (*k-fold CV*) where the training set is randomly divided into k sub-sets or *folds*, of equal length. One of the folds is used as a validation test while the remaining $k - 1$ folds are used for training. This process is repeated k times and for each fold all performance parameters are estimated. An overall performance parameter (specificity, sensitivity, accuracy) is computed by averaging the k estimates of the parameter of interest.

Experimental results

Experimental set up and efficiency

Experimental analyses were carried out to evaluate the proposed method by using the public databases MIAS [12] and DDSM [13] with a MATLAB R2016a implementation. Experiments were executed on a laptop computer with an AMD A10-4600 M processor at 2.3 GHz, and 8 GB RAM. The cross-validation process is 10-fold CV.

Comparison with other methods

Table 3 shows the performance of different methods, including the proposed one, in terms of *TPR* or *sensitivity*, *FPR*, *accuracy* and *AUC* where different public databases are used. The purpose of Table 3 is to show the different databases, and performance measures, used by the scientific community, working on MC detection. Some methods do not report some performance measurements. Our approach achieves the highest metric values in terms of TPR, accuracy and AUC, and it also reaches the lowest FPR values.

Conclusions

Important aspects to the solution of this problem are the reduced number of features (four features), low computational cost, the use of a microcalcification model based on annular regions, features which are independent of image resolution, high performance results. The proposed method promises a good future because of its simplicity for implementation and the advantage of needing a reduced number of features.

The proposed method uses all available mammograms, with MCs, from each database. It also analyzes all the available microcalcifications. To account for FP and TN, normal candidates are randomly generated from the set of MIAS normal images so that the number of ROIs with MC and that of ROIs without MC are equal. Another highlight is the achieved false positive rate in different density mammograms.

The detection of microcalcification candidates, based on the high-pass filter Beucher Gradient, makes the proposed method achieve high performance in detecting microcalcifications on dense mammograms since it locates microcalcifications on areas of low contrast, which is a condition of dense mammograms. Besides, background noise is considerably reduced in dense mammograms and this reduction is higher than that on mammograms with other density type which allows the improvement of feature extraction based on the annulus model.

After comparing the proposed approach with other recent methods, our approach achieves the best performance in terms of *true positive rate* (TPR), *false positive rate* (FPR), *accuracy*, and *area under the ROC curve*; even though other methods are not applied to all available abnormal images, from a database; and the fact that these other works do not specify image selection for experiments. Methods, for MC detection on dense mammograms, show very low performance; however, we give the best performance during MC detection on dense mammograms with 0.9752 for TPR, 0 for FPR, 0.9876 for accuracy, and 0.9951 for AUC. The proposed method outperforms others because of the benefits of using the annulus-based microcalcification model for feature extraction.

Acknowledgements DDSM images are a courtesy of TM Desermo, Dept. of Medical Informatics, RWTH Aachen, Germany". Jonathan Hernández-Capistran likes to thank to Council of Science and Technology (CONACYT) for doctoral scholarship with CVU No. 414681.

Compliance with Ethical Standards

Conflict of Interest Jonathan Hernández-Capistrán declares that he has no conflict of interest. Jorge F. Martínez-Carballido declares that he has no conflict of interest. Roberto Rosas-Romero declares that he has no conflict of interest.

Ethical Approval This article does not contain any studies with human participants performed by any of the authors.

References

1. WHO. WHO | Breast cancer. 2017. *Who*. Retrieved December 18, 2017, from http://www.who.int/cancer/prevention/diagnosis-screening/breast-cancer/en/.
2. Coburn, N. G., Chung, M. A., Fulton, J., and Cady, B., Decreased breast Cancer tumor size, stage, and mortality in Rhode Island: An example of a well-screened population. *Canc. Contrl.* 11(4):222–230, 2004. https://doi.org/10.1177/107327480401100403.
3. Cho, K. R., Seo, B. K., Woo, O. H., Song, S. E., Choi, J., Whang, S. Y., … Chung, H. H. (2016). Breast Cancer detection in a screening population: Comparison of digital mammography, computer-aided detection applied to digital mammography and breast ultrasound. *J. Breast Canc.*, 19(3), 316. doi:https://doi.org/10.4048/jbc.2016.19.3.316
4. Fischer, U., Baum, F., Obenauer, S., Luftner-Nagel, S., von Heyden, D., Vosshenrich, R., & Grabbe, E. (2002). Comparative study in patients with microcalcifications: Full-field digital mammography vs screen-film mammography. *Eur. Radiol.*, 12(11), 2679–2683. doi:https://doi.org/10.1007/s00330-002-1354-x
5. Breastcancer.org. Diagnosis of DCIS. 2015. Retrieved December 18, 2017, from http://www.breastcancer.org/symptoms/types/dcis/diagnosis
6. Pak, F., Kanan, H. R., and Alikhassi, A., Breast cancer detection and classification in digital mammography based on non-subsampled Contourlet transform (NSCT) and super resolution. *Comput. Methods Prog. Biomed.* 122(2):89–107, 2015. https://doi.org/10.1016/j.cmpb.2015.06.009.
7. Institute, N. C. Mammograms. 2016. Retrieved August 8, 2017, from https://www.cancer.gov/types/breast/mammograms-fact-sheet#q1.
8. Dheeba, J., and Selvi, S. T., A swarm optimized neural network system for classification of microcalcification in mammograms. *J.*

Med. Syst. 36(5):3051–3061, 2012. https://doi.org/10.1007/s10916-011-9781-3.

9. Linguraru, M. G., Marias, K., English, R., and Brady, M., A biologically inspired algorithm for microcalcification cluster detection. *Med. Image Anal.* 10(6):850–862, 2006. https://doi.org/10.1016/j.media.2006.07.004.
10. Duarte, M. A., Alvarenga, A. V., Azevedo, C. M., Calas, M. J. G., Infantosi, A. F. C., and Pereira, W. C. A., Evaluating geodesic active contours in microcalcifications segmentation on mammograms. *Comput. Methods Prog. Biomed.* 122(3):304–315, 2015. https://doi.org/10.1016/j.cmpb.2015.08.016.
11. Alasadi, A. H. H., and Al-Saedi, A. K. H., A method for microcalcifications detection in breast mammograms. *J. Med. Syst.* 41(4):1–9, 2017. https://doi.org/10.1007/s10916-017-0714-7.
12. Suckling, J., Parker, J., Dance, D., Astley, S., Hutt, I., Boggis, C., … Savage, J. (1994). The mammographic image analysis society digital mammogram database, *Experta Medica Int. Cong. Ser.*, 1069(JANUARY 1994), 375–378.
13. Heath, M., Bowyer, K., Kopans, D., Moore, R., and Kegelmeyer, P., The digital database for screening mammography. *Proc. Fifth Int. Workshop Digit. Mammograp.*, 212–218. doi:https://doi.org/10.1007/978-94-011-5318-8_75, 2001.
14. Guo, Y., Dong, M., Yang, Z., Gao, X., Wang, K., Luo, C. et al., A new method of detecting micro-calcification clusters in mammograms using contourlet transform and non-linking simplified PCNN. *Comput. Methods Prog. Biomed.* 130:31–45, 2016. https://doi.org/10.1016/j.cmpb.2016.02.019.
15. Vivona, L., Cascio, D., Fauci, F., and Raso, G., Fuzzy technique for microcalcifications clustering in digital mammograms. *BMC Med. Imag.* 14(1):23, 2014. https://doi.org/10.1186/1471-2342-14-23.
16. Mohamed, H., Mabrouk, M. S., and Sharawy, A., Computer aided detection system for micro calcifications in digital mammograms. *Comput. Methods Prog. Biomed.* 116(3):226–235, 2014. https://doi.org/10.1016/j.cmpb.2014.04.010.
17. Chen, Z., Strange, H., Oliver, A., Denton, E. R. E., Boggis, C., and Zwiggelaar, R., Topological modeling and classification of mammographic microcalcification clusters. *IEEE Trans. Biomed. Eng.* 62(4):1203–1214, 2015. https://doi.org/10.1109/TBME.2014.2385102.
18. Ashiru, O., and Zwiggelaar, R., Classification of mammographic microcalcification clusters using a combination of topological and location modelling. *2016 Sixth Int. Conf. Image Process. Theory, Tools Appl. (IPTA)* (pp. 1–6). IEEE. 2016. doi:https://doi.org/10.1109/IPTA.2016.7820986.
19. Hu, K., Yang, W., and Gao, X., Microcalcification diagnosis in digital mammography using extreme learning machine based on hidden Markov tree model of dual-tree complex wavelet transform. *Expert Syst. Appl.* 86:135–144, 2017. https://doi.org/10.1016/j.eswa.2017.05.062.
20. AbuBaker, A. A., Automatic microcalcification detection using wavelet transform. *Int. J. Comput. Theor. Eng.* 7(1):40–45, 2014. https://doi.org/10.7763/IJCTE.2015.V7.927.
21. Muthuvel, M., Thangaraju, B., and Chinnasamy, G., Microcalcification cluster detection using multiscale products based hessian matrix via the Tsallis thresholding scheme. *Pattern Recogn. Lett.*, 2017. https://doi.org/10.1016/j.patrec.2017.05.002.
22. Rivest, J. -F., Soille, P., and Beucher, S., Morphological gradients. In E. R. Dougherty, J. T. Astola, & C. G. Boncelet, Jr. (Eds.), (Vol. 1658, p. 139, 1992. doi:https://doi.org/10.1117/12.58373.